NUCLEAR REACTIONS -- THEORY

SENSITIVITY OF HEAVY-ION CHARGE EXCHANGE TO GAMOW-TELLER STRENGTH

J.S. Winfield, F. Osterfeld,[a] N. Anantaraman, Sam M. Austin, and J.A. Carr[b]

Recently, heavy-ion charge-exchange (HICHEX) reactions such as (^{6}Li,^{6}He), (^{12}C,^{12}B) and (^{12}C,^{12}N) at relatively high bombarding energies have been used to measure Gamow-Teller (GT) transition strengths.[1 – 3] These studies have used phenomenological approaches, and a qualitative theoretical understanding of the relationship between HICHEX cross sections and GT strength has been lacking. A particular concern, arising from the strong absorption present in heavy-ion reactions, is that only the surface parts of the nuclear transition densities are tested in the reactions, or, equivalently, that the transition density is apparently sampled over a large range of the momentum transfer q, so that cross sections might not reflect B(GT), which is given by the square of the transition density at $q \approx 0$. To illustrate this, we plot in Fig. 1 the calculated transition densities for six $0^+ \rightarrow 1^+$ transitions in ^{26}Mg(^{26}Al). While the

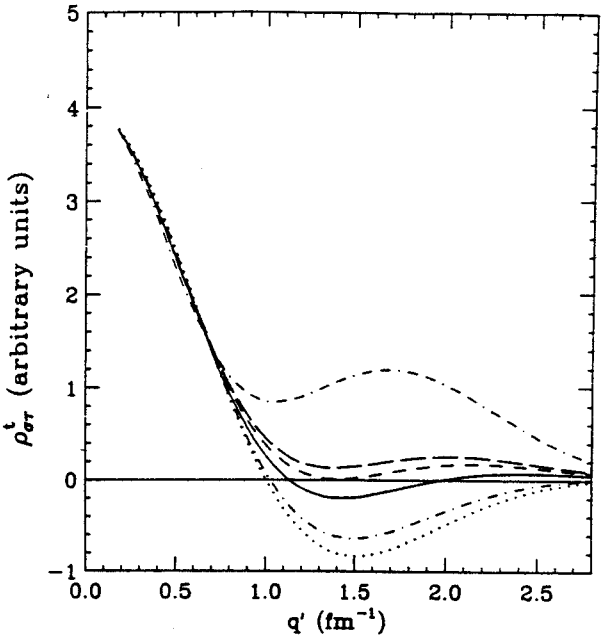

Figure 1: Momentum distributions of the GT transitions densities calculated for the lowest six states of ^{26}Mg $\rightarrow^{26}$ Al(1^+). They are arbitrarily scaled to match at $q' = 0$.

transition densities have similar shapes out to about 0.8 fm^{-1}, there are marked differences at larger q. The strengths of the associated GT transitions also differ by two orders of magnitude. In spite of these differences, detailed Distorted Wave calculations show that HICHEX cross sections *are* closely proportional to B(GT).[3]

We have developed[4] a strong absorption model of HICHEX reactions, along the lines of that

developed by Blair[5] for inelastic alpha scattering. This model makes it possible to examine various terms contributing to the cross section, and to calculate a "sensitivity function" for the target transition density. We assume the beam energy is high enough (> 500 MeV) that the Eikonal approximation can be used and the real part of the optical potential ignored. Because the absorption is strong, the attenuation factor $G(\vec{R})$ in the Eikonal expression for the scattering wave functions, implies that the major contributions to the $\vec{R}$-integration in the transition amplitude are localized in a narrow ring near the strong absorption radius R_0. In our simple model, we consider a square-well optical potential of radius R_0, which results in the following expressions for the differential cross sections due to the central and tensor force terms:

$$\frac{d\sigma}{d\Omega}_{k=0}(\vec{q}) = \left(\frac{\mu}{2\pi\hbar^2}\right)^2 \frac{k_f}{k_i} \mid \int_0^\infty dq' q'^2 V_0(q') \rho^p_{\sigma\tau}(q') \rho^t_{\sigma\tau}(q') G_{00}(q', \vec{q}) \mid^2 \tag{1}$$

$$\frac{d\sigma}{d\Omega}_{k=2}(\vec{q}) = \left(\frac{\mu}{4\pi\hbar^2}\right)^2 \frac{k_f}{k_i} \sum_\nu \mid \int_0^\infty dq' q'^2 V_2(q') \rho^p_{\sigma\tau}(q') \rho^t_{\sigma\tau}(q') G_{2\nu}(q', \vec{q}) \mid^2 \tag{2}$$

where the terms inside the integral are the interaction strength V_k, the projectile and target transition densities $\rho^p_{\sigma\tau}$ and $\rho^t_{\sigma\tau}$, and

$$G_{k\nu}(q', \vec{q}) = \frac{\delta(q - q')}{qq'} Y^*_{k\nu}(\hat{q}) + F^{k\nu}_1(q', \vec{q}) - F^{k\nu}_2(q', \vec{q}). \tag{3}$$

The three terms in Eq. (3) consist of: (i) a δ-function term which produces a plane wave transition amplitude; (ii) a term $F^{k\nu}_1$ which is governed by the attenuation factor $G(\vec{R})$ and describes the scattering from an absorbing sphere of radius R_0; and (iii) a term $F^{k\nu}_2$ which describes the scattering from a bright sphere of the same radius R_0, and is *subtracted* from the other two wave amplitudes. The $F^{k\nu}$ functions are essentially proportional to the spherical Bessel functions $j_0(q'R)$ and $j_2(q'R_0)$ in the central and tensor case, respectively. The weighting with the tensor force, which increases with increasing q', and with $j_2(q'R_0)$, which peaks at $q' > 0$, explains why the cross section contribution of this force to GT states is relatively large in HICHEX reactions.

The model has been compared with data from Ref. 3, and the $L = 0$ (central) part of the calculated cross section found to a fair description of the shape and strength of the data. In Fig. 2, we plot a sensitivity function $S(q')$,

$$S(q') = q'^2 V_0(q') \rho^p_{\sigma\tau}(q') G_{00}(q', 0), \tag{4}$$

the product of the important terms in the expression for the cross section (omitting the target transition density, $\rho^t_{\sigma\tau}(q')$), as a function of q' for $q = 0$. The sensitivity function has a peak at $q' = 0.4$ fm^{-1} and

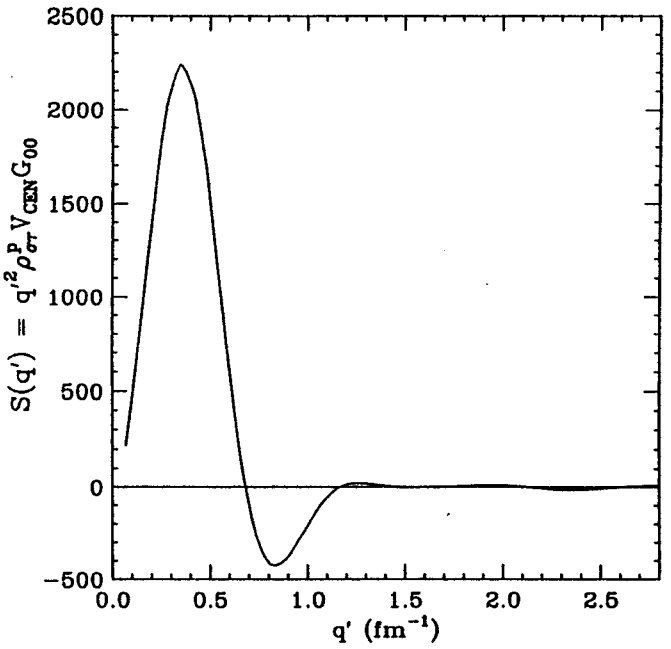

Figure 2: The product of the terms in the expression for the $L = 0$ cross section, excluding $\rho^t_{\sigma\tau}(q')$, plotted as a function of q' at $q = 0$.

a FWHM of about 0.45 fm^{-1}. As a result, the reaction is insensitive to $q' \geq 0.8$ fm^{-1} and the target transition densities are sampled in the region where they are similar in shape (compare Fig. 1). Thus the $L = 0$ cross section will be proportional to the value of $\rho^t_{\sigma\tau}(0)$, and therefore B(GT), in a similar way from state to state. This important result justifies the use of heavy ion reactions, even with the accompanying strong absorption, for the measurement of GT strength. If one can determine the $L = 0$ cross section in the presence of significant $L = 2$ contributions, HICHEX reactions can serve to determine GT strength without large model dependence. Multipole decompositions have been used successfully for this purpose.[3]

a. Institut für Kernphysik, Jülich, Germany.
b. SCRI, Florida State University, Tallahassee, FL.

References

1. H. Wirth, E. Aschenauer, W. Eyrich, A. Lehmann, M. Moosburger, H. Schlösser, H.J. Gils, H. Rebel, and S. Zagromski, Phys. Rev. C 41, 2698 (1990).
2. S. Nakayama, T. Yamagata, M. Tanaka, M. Inoue, K. Yuasa, T. Itahashi, H. Ogata, N. Koori, and K. Shima, Phys. Rev. Lett. 67, 1082 (1991).
3. N. Anantaraman, J.S. Winfield, S.M. Austin, J.A. Carr, C. Djalali, A. Gillibert, W. Mittig, J.A. Nolen, Jr., and Z.W. Long, Phys. Rev. C 44, 398 (1991).
4. F. Osterfeld, N. Anantaraman, Sam M. Austin, J.A. Carr, and J.S. Winfield, Phys. Rev. C 45 2854 (1992).
5. J.S. Blair, Phys. Rev. 115, 928 (1959); Lectures in Theoretical Physics, Boulder, ed. by P.D. Kunz, (Gordon and Breach, Sci. Publ., 1965).

BUBBLE AND RING FORMATION IN NUCLEAR FRAGMENTATION

Wolfgang Bauer, George F. Bertsch, and Hartmut Schulz

At sufficiently high excitation energies ($E^*/A > 10$ MeV) of nuclear matter, copious production of intermediate mass fragments is observed. This excitation energy can be deposited in different ways. The two most common are: 1) Bombardment of heavy target nuclei with very high energy protons (or the same process in reverse kinematics), and 2) Central collisions of target and projectile with approximately equal mass numbers at intermediate beam energies ($E/A \approx 50$ MeV).

The first type of reaction is assumed to be a two-step process. In the first step, the small projectile only interacts with the target nucleons in its direct path; some of the sideways ejected nucleons and pions penetrate into the spectator matter and give rise to its excitation. In the second step, the excited target spectator matter decays.

Central heavy ion reaction proceed in a different way: In the initial state of the reaction, thermalization takes place via binary nucleon-nucleon collisions. During this stage the nuclei compress each other, whereby typical densities of $\rho/\rho_0 \approx 1.3$-1.5 are reached. This excited and compressed participant matter then expands and decays.

The reaction mechanism, via which intermediate mass fragments are formed, is still debated. At lower excitation energies, sequential emission from the surface in a statistical fashion is dominant. At higher energies simultaneous multifragmentation of the entire nuclear volume seems to be favored Since the nuclear interaction exhibits short range repulsion and intermediate range attraction, the resulting nuclear equation of state exhibits a phase transition between the liquid-like and gas-like phases. The phenomenon of multifragmentation has been connected to this effect. Of the phase transition models under consideration so far, percolation based models have been most successful in reproducing high-energy proton-induced and light-ion-induced multifragmentation data.[1,2]

Here we propose a novel path leading to the emission of intermediate mass fragments in heavy ion collision: The formation of unstable hollow bubbles and rings of nuclear matter, which decay by fragment emission.[3] Our reasoning is based on the numerical solution of the nuclear Boltzmann-Uehling-Uhlenbeck transport equation.[4,5]

To illustrate the occurrence of the bubble and ring structures, we show in Fig. 1 the time evolution

Nb + Nb, E/A = 60 MeV, b = 0 fm

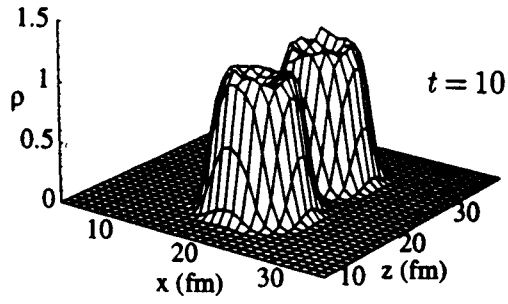

$t = 10$ fm/c

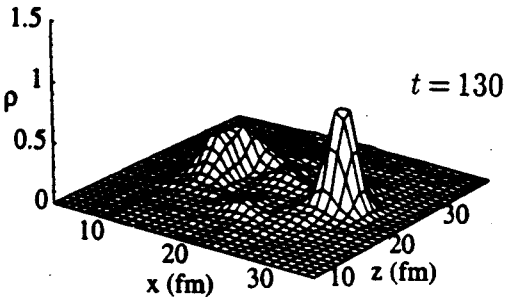

$t = 130$ fm/c

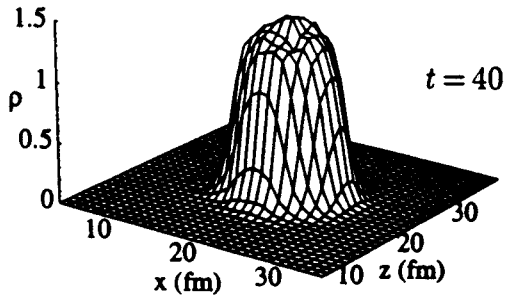

$t = 40$ fm/c

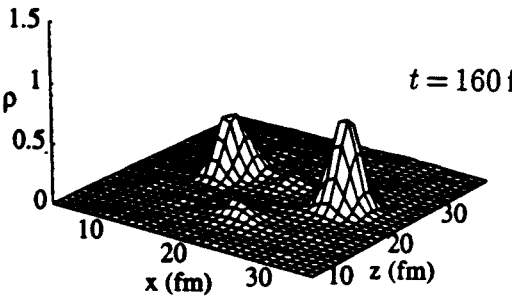

$t = 160$ fm/c

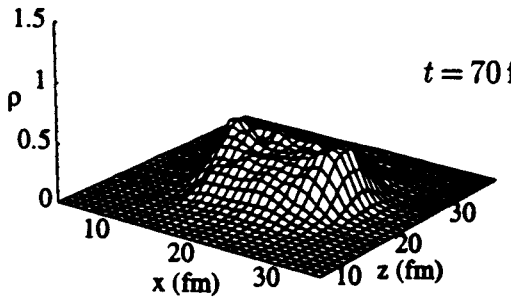

$t = 70$ fm/c

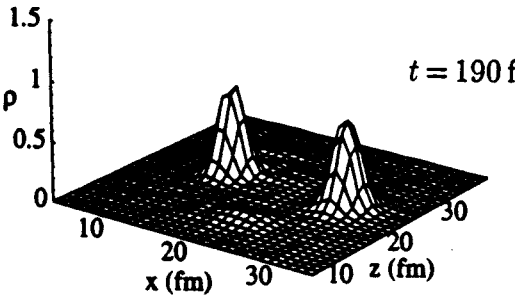

$t = 190$ fm/c

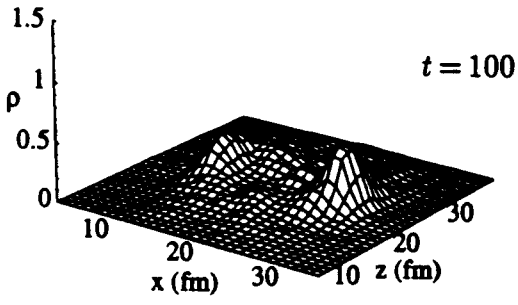

$t = 100$ fm/c

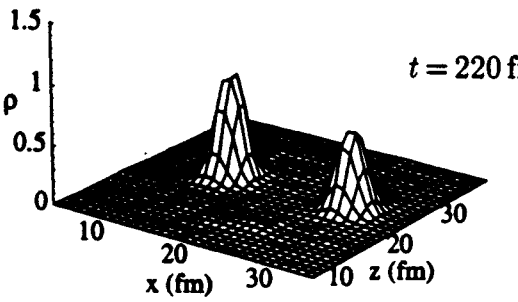

$t = 220$ fm/c

of a central ^{93}Nb+^{93}Nb collision at E_{beam}/A = 60 MeV. We display the nucleon density in the reaction plane for different times during the reaction. In the early phase (t = 40 fm/c) of the reaction, the two nuclei compress each other in their overlap zone to a density of $\rho \approx 1.4\,\rho_0$, and the density distribution is approximately spherically symmetric.

The transiently compressed system expands radially, and the central density falls to a value below $\rho_0/2$. The bulk of the matter forms a spherical shell.

The occurrence of this striking feature is sensitively dependent on the amount of radial kinetic energy supplied by the initial compression. At higher beam energies, the initial compression is increased, and the energy of radial expansion exceeds the nuclear binding energy. Then the result is a prompt disintegration of the entire nuclear volume. At lower beam energies, the initial compression is too small, and monopole type oscillations are the consequence. Since the initial compression is dependent on the nuclear incompressibility, the occurrence of the shapes predicted by us may also yield valuable information on this key parameter of the nuclear equation of state.

We can see from Fig. 1 that the bubble shaped nuclear remnant is converted into a ring (or doughnut) shaped object during the subsequent time evolution, as indicated by the two bumps in the density distribution in the reaction plane (t = 160 fm/c).

The doughnut shape reflects an imbalance towards sidewards flow in the nearly-symmetric compressed phase. The bubble shape would be preserved to longer times for a lighter mass system, since that would equilibrate slightly later.

We predict two major experimental consequences of the bubble and ring formation. First there should be more intermediate mass fragments formed from these extended systems than would be produced by the decay of a compact object at the same temperature. It is difficult to quantify this tendency, but it is clear that a relatively cool object with a large surface will produce more fragments than a hot object with a smaller surfaces, which will emit mainly neutrons and hydrogen and helium isotopes.

The second prediction is that the Coulomb acceleration in the final state will on average be smaller than expected from the decay of a uniform density spherical system. Generally, one fits the spectra assuming a distribution of Coulomb barriers as the decay proceeds, and the average barrier will be reduced. If non-compact topological objects are formed transiently, the barrier reduction will be stronger

than that from a volume break-up.

There is another small Coulomb effect that may be observable. In volume decays, a small fraction of the fragments originate at the center and are not subject to Coulomb acceleration. This fraction will no longer be present here, because the center is empty. All the fragments are at roughly a common radius.

References

1. W. Bauer *et al.*, Phys. Lett. 150B, 53 (1985); Nucl. Phys. A452, 699 (1986); W. Bauer, Phys. Rev. C 38, 1927 (1988).
2. X. Campi, Phys. Lett. 351B, 208 (1988).
3. W. Bauer, G.F. Bertsch, and H. Schulz, submitted to Phys. Rev. Lett.
4. G.F. Bertsch, H. Kruse, and S. Das Gupta, Phys. Rev. C 29, 673 (1984); G.F. Bertsch and S. Das Gupta, Phys. Rep. 160, 189 (1988).
5. W. Bauer *et al.*, Phys. Rev. C 34, 2127 (1986); W. Bauer, Phys. Rev. Lett. 61, 2534 (1988); W. Bauer, C.K. Gelbke, and S. Pratt, Annu. Rev. Nucl. Part. Sci. 42, 77 (1992).

NUCLEAR DYNAMICS AND INTENSITY INTERFEROMETRY

Wolfgang Bauer

Koonin[1] proposed to use two-proton intensity interferometry to obtain 'pictures' of heavy ion collisions. The advantage of using protons as a probe lies in the fact that they are already present in the colliding nuclei and can be liberated relatively easily. In contrast, to create a pair of pions one has to spend an energy $E_{\rm min} = 2\,m_\pi \approx 280$ MeV in the center of mass of the generating system. Therefore, protons can be used as a probe at much lower energies. In addition, the two-proton relative wave function contains the prominent ^{2}He-'resonance', which leads to enhanced sensitivity of the correlation function to the source size. Lastly, protons are easy to detect with the required resolution.

Recent progress has been centered around the theoretical computation of two-proton correlation functions from nuclear transport theory.[2] In this framework, it is now possible to understand the dependence of the correlation functions on the mass and beam energy of the emitting system, on the velocity of the emitted pair, and on the relative momentum between the two particles.

To derive an expression for the two-particle correlation function, $C(\vec{P},\vec{q})$, we assume that the final-state interaction between the two detected particles dominates, that final-state interactions with all remaining particles can be neglected, that the correlation functions are determined by the two-body density of states as corrected by the interactions between the two particles, and that the single particle phase space distribution function of emitted particles, $g(\vec{p},x)$ varies slowly as a function of momentum $\vec{p}$ (i.e. $g(\vec{p},x) \approx g(\vec{p}\pm\vec{q},x)$). Then the theoretical expression for the two-particle correlation function can be written as[1,2]

$$C(\vec{P},\vec{q}) = R(\vec{P},\vec{q}) + 1 = \frac{\Pi_{12}(\vec{p}_1,\vec{p}_2)}{\Pi_1(\vec{p}_1)\Pi_1(\vec{p}_2)}$$

$$= \frac{\int d^4x_1 d^4x_2\, g(\frac{1}{2}\vec{P},x_1) g(\frac{1}{2}\vec{P},x_2) \left|\phi\left(\vec{q},\vec{r}_1-\vec{r}_2+\frac{\vec{P}(t_2-t_1)}{2m}\right)\right|^2}{\int d^4x_1\, g(\frac{1}{2}\vec{P},x_1) \int d^4x_2\, g(\frac{1}{2}\vec{P},x_2)}\,, \qquad (1)$$

where $\vec{P} = \vec{p}_1 + \vec{p}_2$ and $\vec{q} = (\vec{p}_1 - \vec{p}_2)/2$ are the total and relative momentum of the particle pair. x_1 and x_2 are the space-time points of the emission of protons 1 and 2. Π_1 is the single- and Π_{12} is the two-particle emission probability.

$\phi(\vec{q},\vec{r})$ is the relative wave function of the particle pair. The effect that gives rise to the HBT effect is the identical particle interference. In the absence of any other interaction the square of the two particle wave function is then simply given by

$$|\phi(\vec{q},\vec{r})|^2 = 1 \pm \cos(2\vec{q}\,\vec{r}) \,, \tag{2}$$

where the upper sign stands for bosons and the lower for fermions. To solve the two-proton problem, the relative wave function has to also include the contributions from the Coulomb and strong interaction of the two protons.

Equation 1 requires only the two-particle relative wave function and the *single*-particle phase space distribution function. Under the assumptions stated above it is thus possible to generate *two*-particle correlation functions for small relative momenta from a theory which only predicts *one*-particle distribution functions.

The resulting two-particle correlation function contains information on the emitting source. To see this, we rewrite Equation 1 as

$$C(\vec{P},\vec{q}) = \int d^3r\, F_{\vec{P}}(\vec{r})\, |\phi(\vec{q},\vec{r})|^2 \,. \tag{3}$$

Here $\vec{r} = \vec{r}_1 - \vec{r}_2$ is the relative coordinate of the two emitted particles, and the function $F_{\vec{P}}(\vec{r})$ is defined as

$$F_{\vec{P}}(\vec{r}) = \frac{\int d^3R\, f(\frac{1}{2}\vec{P},\vec{R}+\frac{1}{2}\vec{r},t_>) f(\frac{1}{2}\vec{P},\vec{R}-\frac{1}{2}\vec{r},t_>)}{\left(\int d^3r f(\frac{1}{2}\vec{P},\vec{r},t_>)\right)^2} \,, \tag{4}$$

where $\vec{R} = \frac{1}{2}(\vec{r}_1 + \vec{r}_2)$ is the center-of-mass coordinate of the two particles, and the Wigner function $f(\vec{p},\vec{r},t_>)$ is the phase space distribution of particles with momentum $\vec{p}$ and position $\vec{r}$ at some time $t_>$ after both particles have been emitted:

$$f(\vec{p},\vec{r},t_>) = \int_{-\infty}^{t_>} dt\, g(\vec{p},\vec{r}-\vec{p}(t_>-t)/m,t) \,. \tag{5}$$

For a given momentum $\vec{P}$, the correlation function has three degrees of freedom, $\vec{q}$, which are a function of $F_{\vec{P}}(\vec{r})$.

The phase space distribution function f of the emitted protons is in our approach obtained from

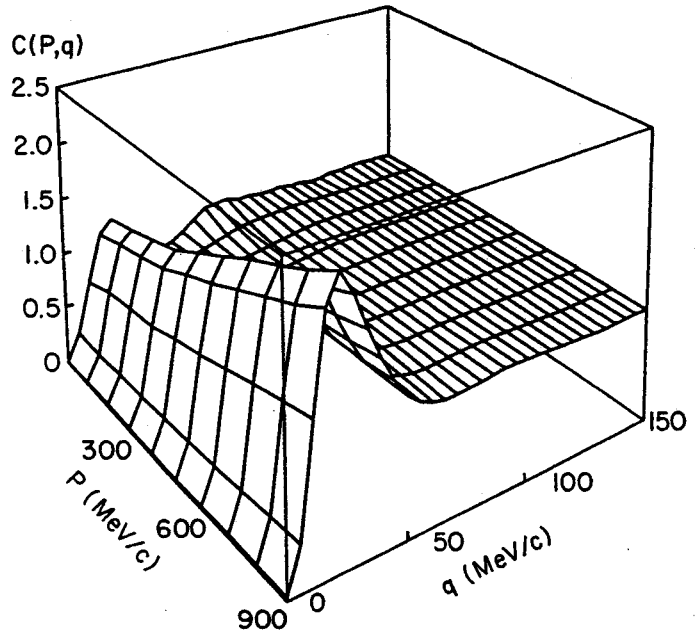

Figure 1: Two-proton correlation function as a function of the absolute value of total pair momentum, P, and relative momentum, q, for the reaction ^{14}N + ^{27}Al at beam energy E/A = 75 MeV and impact parameter b = 0 fm.

the solution of the nuclear Boltzmann-Uehling-Uhlenbeck (BUU) transport equation

$$\begin{aligned}\frac{\partial}{\partial t}f(\vec{r},\vec{p},t) \;+\; & \frac{\vec{p}}{m}\vec{\nabla}_r f(\vec{r},\vec{p},t) - \vec{\nabla}_r U\,\vec{\nabla}_p f(\vec{r},\vec{p},t) \\ = \; & \frac{g}{2\pi^3 m^2}\int d^3q_{1'}\,d^3q_2\,d^3q_{2'} \\ & \delta\left(\frac{1}{2m}(p^2+q_2^2-q_{1'}^2-q_{2'}^2)\right)\cdot\delta^3(\vec{p}+\vec{q}_2-\vec{q}_{1'}-\vec{q}_{2'})\cdot\frac{d\sigma}{d\Omega} \\ & \cdot\Big\{f(\vec{r},\vec{q}_{1'},t)\,f(\vec{r},\vec{q}_{2'},t)\left(1-f(\vec{r},\vec{p},t)\right)\left(1-f(\vec{r},\vec{q}_2,t)\right) \\ & -f(\vec{r},\vec{p},t)\,f(\vec{r},\vec{q}_2,t)\left(1-f(\vec{r},\vec{q}_{1'},t)\right)\left(1-f(\vec{r},\vec{q}_{2'},t)\right)\Big\},\end{aligned} \tag{6}$$

Here U is the mean field potential, and $d\sigma/d\Omega$ is the in-medium nucleon-nucleon scattering cross section.

We perform calculations of the single particle phase space distribution function $f(\vec{r},\vec{p},t)$ by numerically solving Equation 6. These single particle distributions are then inserted into Equation 1 to generate the two-particle correlation function at small relative momentum.

In Figure 1, we show the two-proton correlation function, $C(P,q)$, calculated for the reaction ^{14}N + ^{27}Al at beam energy E/A = 75 MeV and impact parameter b = 0 fm. We can clearly observe the suppression of the correlation function at $q \approx 0$ due to the combined effects of Coulomb interaction and

antisymmetrization.. Also clearly visible is the enhancement of the correlation function around q = 20 MeV/c due to the ^{2}He resonance. One can see that the height of the resonance peak varies with total momentum, P. This effect is also experimentally observed. When fitting a source radius to the correlation function one then observes a typical momentum dependence of the extracted source size.[3]

We have therefore shown that it is indeed possible to take 'proton pictures' of heavy ion collisions, but that the image obtained is dependent on the velocity of the emitted pair.

References

1. S.E. Koonin, Phys. Lett. 70B, 43 (1977).
2. W.G. Gong, *et al.*, Phys. Rev. Lett. 65, 2114 (1990); W.G. Gong, W. Bauer, C.K. Gelbke, and S. Pratt, Phys. Rev. C 43, 781 (1991); W.G. Gong, *et al.*, Phys. Rev. C 43, 1804 (1991).
3. W. Bauer, C.K. Gelbke, and S. Pratt, Ann. Rev. Nucl. Part. Sci. 42 (1992).

COLLECTIVE PION FLOW?

Bao-An Li, Wolfgang Bauer, and George F. Bertsch

Looking for flow signatures among pions, several groups[1-3] have studied the transverse momentum distribution in the reaction plane ($\langle p_x \rangle$ versus rapidity y) for pions. One of the most striking results from the DIOGENE collaboration[1] is that the in-plane transverse momentum of pions is always positive even for backword rapidities, for the asymmetric (Ne or Ar) + (Nb or Pb) systems.

Here we report on the results of a study using a hadronic transport model.[4] The calculations were perfomed by numerically solving a coupled set of transport equations for the phase space distribution functions of nucleons, Deltas and pions. The preferential emission of pions towards the projectile side in the transverse direction in the reaction Ne + Pb at a beam energy of 800 MeV/nucleon is found to be due to the stronger absorption of pions by the heavier target spectator. The calculated transverse momentum distribution of pions in the reaction plane agrees with that of the experimental data.[5]

Is the nonzero in-plane transverse momentum of pions a remnant of the baryon collective flow carried by Δ resonances? To answer this question we have studied the dependence of the pion transverse momentum distribution on the nuclear equation of state. Within statistical fluctuations, results from the calculations done with a stiff equation of state corresponding to the nuclear compressibility of K = 380 and with a soft equation of state corresponding to K = 210 are the same. This indicates that the effect of baryon collective flow on the pion transverse momentum distribution is negligible and the origin of the positive in-plane transverse momentum of pions is not predominantly the remnant of the Δ flow.

To study the effect of the pion reabsorption and rescattering and therefore check the shadowing effect in forming the positive in-plane transverse momentum of pions, we calculated the pion transverse momentum distribution and the rapidity distribution by turning off the pion reabsorption channels and the Δ rescattering channel. In this case the in-plane transverse momentum is zero within statistical error bars and the rapidity distribution is symmetric about half-beam rapidity of 0.6 unit, which reflects the fact that the pions are emitted isotropically in the center of mass frame of two colliding nucleons.

In order to compare the model predictions and the experimental data of the pion transverse momentum distribution, we have made a full simulation of the detector acceptance of the DIOGENE collaboration. In the same way as in the experimental data analysis,[1] we estimate the reaction plane for

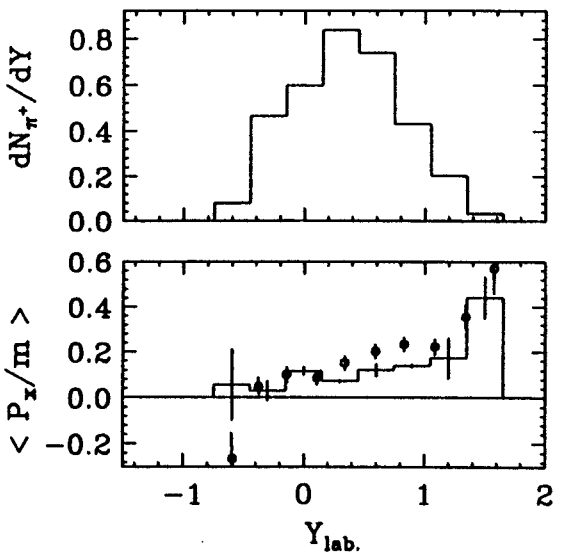

Figure 1: Upper figure: calculated π^+ rapidity distribution after using the detector filter cut for the Ne + Pb reaction at E/A = 800 MeV. Lower figure: Comparision between the experimental pion transverse momentum distribution (round plot symbols) and the model calculation (histogram) for the same reaction.

each event from the beam direction and the vector

$$\vec{Q}_j = \sum_{i \neq j} w_i \vec{p}_{\perp i} \tag{1}$$

determined from the detected protons. Here the weights are $w_i = y_i - \bar{y}$, and $\bar{y}$ is the average rapidity of the detected protons. These weights are different from the ones originally proposed for symmetric systems, since the center of mass rapidity of the participant system is not known *a priori* in each event for asymmetric nucleus-nucleus collisions. The transverse momentum of a particle j in the estimated reaction plane is defined as

$$p_{xj} = \left\{ \vec{Q}_j \cdot \vec{p}_{\perp j} / |\vec{Q}_j| \right\}. \tag{2}$$

In Fig. 1, we perform a comparison between the experimental data and the model calculations for the Ne + Pb reaction. The experimental data are represented by the round plot symbols. The solid histograms are the model calculations, the error bars in the model calculations are statistical in nature, since we solve the coupled transport equations for the hadronic matter with a Monte Carlo integration technique. The experimental data are in reasonable agreement with our model predictions. To show the effect of the detector filter cut, the rapidity distribution of the detected π^+'s in the model calculation has been shown in the upper part of Fig. 1.

From the results of our calculations, it is clear that the positive in-plane transverse momentum of pions in the asymmetric nucleus-nucleus collisions is due to the stronger reabsorption of pions by the heavier target.

References

1. J. Gosset *et al.*, Phys. Rev. Lett. 62, 1251 (1989).
2. D. Keane, D. Beavis, S.Y. Chu, S.Y. Fung, W. Gorn, Y.M. Liu, G. VanDalen and M. Vient, in Proceedings of the 4^{th} Nuclear Dynamics Workshop, Copper Mountain, Colorado, 1986, p.151.
3. P. Danielewicz *et al.*, Phys. Rev. C 38, 120 (1988).
4. B.A. Li and W. Bauer, Phys. Lett. B254, 335 (1991); S.J. Wang, B.A. Li, W. Bauer and J. Randrup, Ann. of Phys. (N.Y.) 209, 251 (1991); B.A. Li and W. Bauer, Phys. Rev. C 44, 450 (1991).
5. B.A. Li, W. Bauer, and G.F. Bertsch, Phys. Rev. C 44, 2095 (1991).

FRAGMENT PRODUCTION FROM A SURFACE EMISSION MODEL

C. M. Mader, W. Bauer, and W. A. Friedman[a]

Recent experiments[1] have measured intermediate mass fragment (IMF) production for reactions of 50 MeV/A Xe + X. In central collisions, they have measured as many as 14 IMFs in a single event. Comparisons of their results with standard statistical decay models underpredict this number. However, the rapid massive cluster formation (RMCF) model[2] of Friedman was able to reproduce the experimental results. In this statistical model, the hot residual nucleus formed during the collision is allowed to expand while emitting fragments and particles from its surface.

The model requires 5 input parameters: mass (A), radius (R), radial expansion energy (E_r), temperature (T), and compressibility (K). In order to determine whether the input values necessary to reproduce the data were reasonable, we use a heavy ion transport model[3] which solves the Boltzmann-Uehling-Uhlenbeck equation using the test particle method. In this single particle model, the nucleons follow classical equations of motion under the influence of a nuclear mean field while experiencing two-body collisions. The Pauli principle is enforced by blocking of collisions where the final states are occupied.

Due to its single particle formalism, the BUU model is unable to predict IMF production. However, it is reliable for modeling the first ~ hundred fm/c of the collision during which the hot residual nucleus is formed. For this reason, we use the BUU transport model to simulate the initial stages of the collision. We use this model to determine

$$A_{res} = \sum_i 1 \tag{1}$$

$$R = R_{rms} = \sqrt{\frac{\sum_i r_i^2}{A_{res}}} \tag{2}$$

$$E_r = \frac{1}{2} m \dot{R}_{rms}^2 = \frac{(\sum_i \vec{r}.\vec{p})^2}{2mR_{rms}^2} \tag{3}$$

$$T = \frac{2E^*}{3A_{res}} = \frac{2(\sum_i (\frac{p_i^2}{2m} + U_i) - E^\circ_{bind})}{3A_{res}} \tag{4}$$

where we sum over all test particles in the residue. U is the potential energy and E°_{bind} is the binding energy of a ground state nucleus of mass A_{res}. We will then use the RMCF model to calculate the statistical decay of the residue while allowing it to continue to expand.

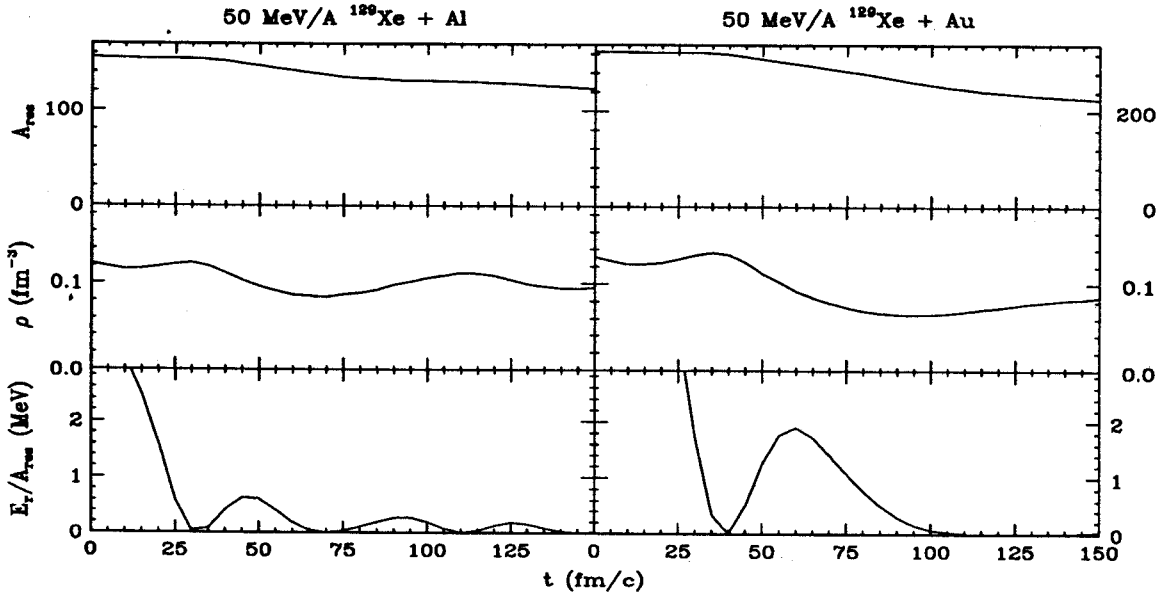

Fig. 1: Mass, density and radial kinetic energy per particle of the residue in 50 MeV/A ^{129}Xe + Al, Au. These calculations were done using the BUU code with a stiff equation of state (K=380 MeV).

Figure 1 shows the results of the BUU calculations as a function of time for central collisions of 50 MeV/A ^{129}Xe on Al and Au. In this case we used a stiff equation of state (EOS) which corresponds to a compressibility K = 380 MeV. In these calculations, the particles were considered to be part of the residue if the local density was greater than $\frac{1}{8}\rho_o$. The surfaces of the nuclei are initially separated by 4 fm. At $\approx$ 25 fm/c, the two surfaces begin to touch, the nuclei begin to compress and the density starts to increase. After the initial compression, the nuclei expand and particles begin to leave the residue. At some point, the nuclear attraction takes over and the residue begins to compress again. This is most obvious in the Al case where several oscillations are seen during the first 150 fm/c.

Some time instance between the first maximum and minimum in the density of the residue provides the initial condition for the RMCF calculation. The RMCF model assumes a uniform density distribution at normal nuclear matter density for the residue. In figure 2 we show $\rho(R)$ at several times produced by the BUU calculation. We chose the RMCF initial time as the instant when the central density returns to normal nuclear matter density. For the Al target, this time is chosen as 45 fm/c while for the Au target it is 55 fm/c.

One other complication is the definition of bound and unbound particles. Even though the local density can be greater than $\frac{1}{8}\rho_o$, particles may have outward velocities high enough for them to be unbound and thus should not be considered part of the residual nucleus. To determine the radius of the residue

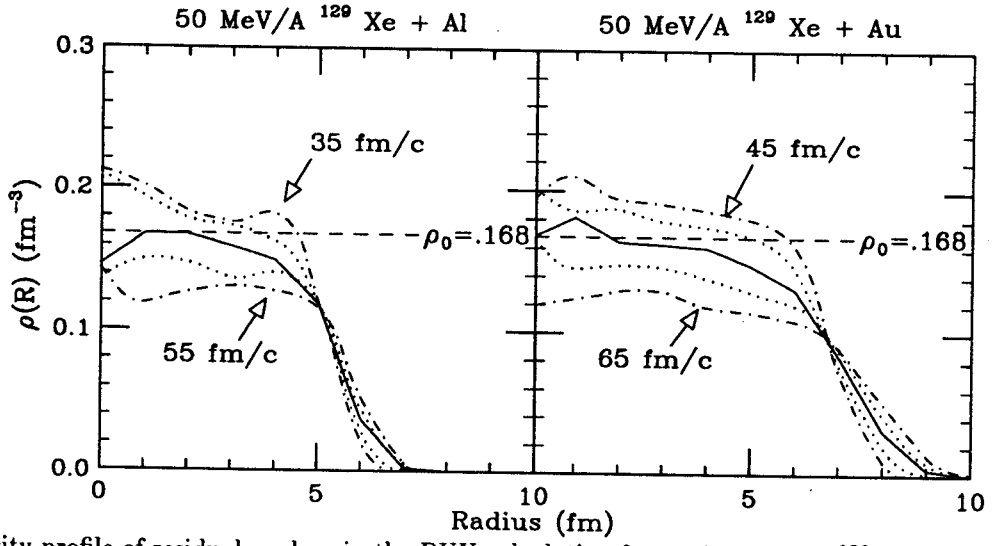

Fig. 2: Density profile of residual nucleus in the BUU calculation for a stiff EOS for ^{129}Xe + Al, Au. Each line corresponds to a different time, with time steps of 5 fm/c. For example, the upper dash-dotted line in the left figure corresponds to 35 fm/c, the next line (dotted), to 40 fm/c, the solid to 45 fm/c, etc.

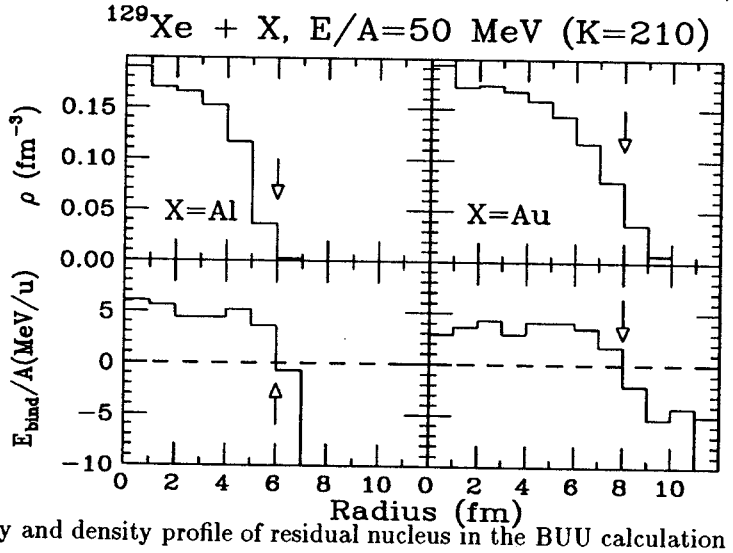

Fig. 3: Binding energy and density profile of residual nucleus in the BUU calculation for a soft EOS for ^{129}Xe + Al, Au.

to use in the RMCF model, we calculated the binding energy per nucleon as a function of radius. This is shown in figure 3 with the density profile at the change over time. In this calculation we used a soft EOS corresponding to K = 210 MeV. All particles inside 8 fm have negative total energy and are considered part of the residue. We also ran the calculations with a cut-off radius 1 fm larger to see how this affects the results.

Figure 4 shows the data for the two target-projectile combinations. The enclosed regions with vertical lines are the unfiltered results of the hybrid model for various cut-off radii and compressibilities. The enclosed regions with horizontal lines are the filtered results. The two different regions are a

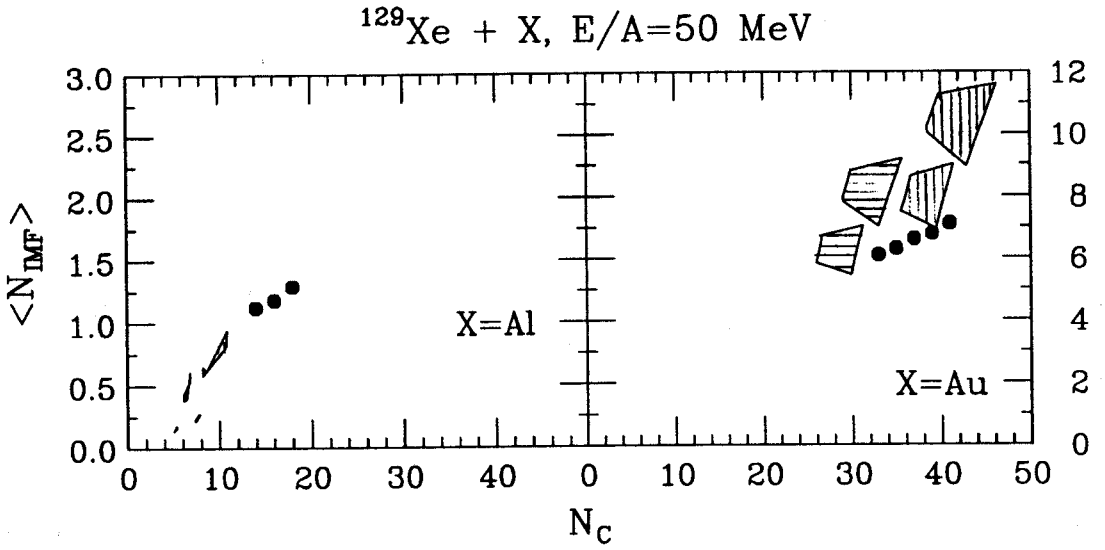

Fig. 4: Charged particle multiplicities vs. average number of IMFs for ^{129}Xe + Al and Au. The boxed regions represent model predictions for various radius cuts and compressibilities. In each plot, the right set of boxes are unfiltered results and the left set are filtered with experimental efficiency cuts.[4]

result of increasing the radius cut by 1 fm. This had the effect of increasing the mass and excitation energy of the residue, thus decreasing the number of IMFs produced in the RMCF model. Varying the compressibility parameter in the BUU calculation, creates the horizontal widths of the regions (the lower compressibility corresponds to the left side of the region), while the vertical spread is a result of changing the compressibility parameter in the RMCF code (the lower compressiblity corresponds to the top of the region). The sensitivity of the model calculations to the various radius cut-offs and compressibilities will not allow precise determination of these parameters. However, the fact that the RMCF model is able to produce enough IMFs with reasonable input variables as determined by the BUU model suggests that expansion of the residue is necessary to explain the observed IMF multiplicities.

a. Dept. of Physics, Univ. of Wisconsin, Madison, WI53706, USA.

References

1. D. R. Bowman, *et al*, Phys. Rev. Let. 67 (1991) 1527.
2. W. A. Friedman, Phys. Rev. C 42 (1990) 667.
3. W. Bauer, *et al*, Annu. Rev. Nucl. Part. Sci. 42 (1992) 77, and references therein.
4. D. R. Bowman, *et al*, submitted to Phys. Rev. C.

FLOW EXCITATION FUNCTION

Dietrich Klakow, Gerd Welke and Wolfgang Bauer

We are studying flow production in nuclei with a finite surface. Flow strongly depends on the surface and in calculations of E_{Bal} (the zero of the flow excitation function) it is as important as the choice of the equation of state.[3] The surface dependence of flow can be understood in terms of a toy model.[1] Let us assume, that at high energies the nuclei basically pass through each other without changing their shape. Then the center of mass of the nuclei move according to the hamilton function

$$H = \frac{p_1^2}{2m_1} + \frac{p_2^2}{2m_2} + \tilde{V}(R) \tag{1}$$

where the potential is given by

$$\tilde{V}(R) = \int \frac{A}{2}\frac{\rho(\vec{r})^2}{\rho_0} + \frac{B}{\sigma+1}\frac{\rho(\vec{r})^{\sigma+1}}{\rho_0^\sigma} dr^3. \tag{2}$$

To describe nuclei with a surface, we choose the density to be

$$\frac{\rho_R(r)}{\rho_0} = \frac{1}{1+\exp\left(|\vec{r}-\frac{\vec{R}}{2}|-R_0\right)/a} + \frac{1}{1+\exp\left(|\vec{r}+\frac{\vec{R}}{2}|-R_0\right)/a}, \tag{3}$$

where R_0 is the radius of the nucleus, $4a$ is the surface thickness and R the separation of the nuclei. As

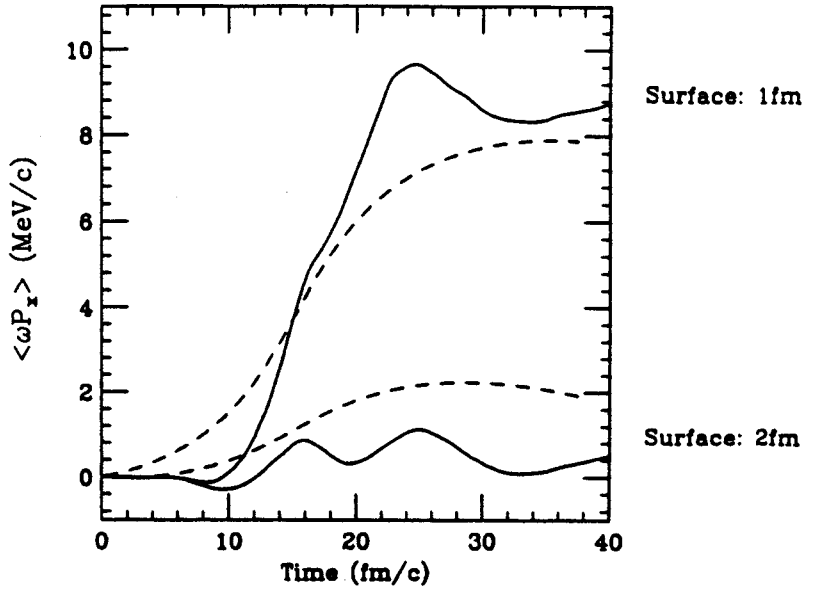

Figure 1: The time evolution of flow for a La on La collision in pure Vlasov dynamics (solid line) and the toy model (dashes) for a surface thickness of 1 fm (upper two lines) and 2 fm (lower two lines).

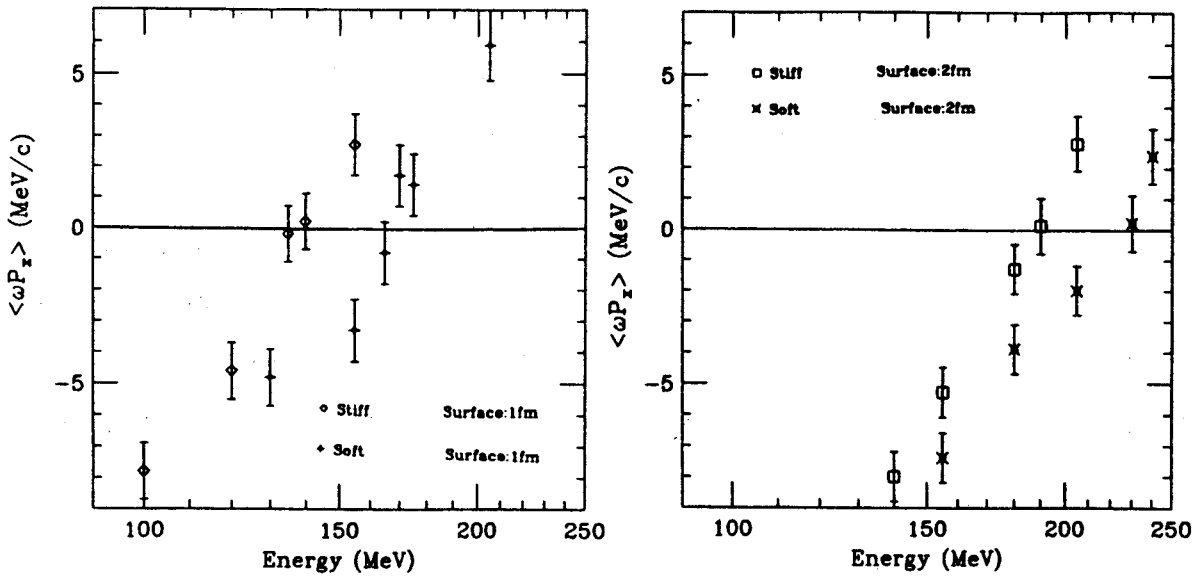

Figure 2: Disappearance of flow for C on C at b=1.41 fm. The left panel is for a surface of 1 fm, the right panel for a surface of 2 fm. Both give results for stiff (open symbols, upper line) and soft equation of state (lower line).

the surface thickness increases, the potential decreases. Hence we expect a larger surface to produce less flow. This can be checked in the time evolution of flow as shown in Fig. 1. We compare the toy model with a Vlasov calculation and find reasonable agreement. Of course, some details are different due to the crude assumptions made in the toy model. For example, the toy model shows no zeros in the flow excitation function, while for the Vlasov calculation E_{Bal} occurs between 200 MeV and 300 MeV, depending on the surface. The surface dependence becomes even more obvious in the C on C system, which recently has been measured at the NSCL.[2] We now do a full BUU calculation by switching on the collisions. Fig. 2 shows the calculated disappearance of flow for a surface of 1 fm (stiff EOS gives $E_{Bal} \approx 140$ MeV and soft EOS gives $E_{Bal} \approx 170$ MeV) and a surface of 2 fm ($E_{Bal} \approx 190$ MeV and $E_{Bal} \approx 220$ MeV for stiff and soft EOS, respectively). We again see the importance of the surface thickness. The use of a momentum dependent mean field and local Thomas-Fermi approximation for momentum space initialization will also influence the balance energy.

References

1. C. Gale, G.M. Welke, M. Prakash, S.J. Lee, and S. Das Gupta, Phys. Rev. C 41, 1545 (1990).
2. G.D. Westfall et al., submitted to Physical Review Letters.
3. D. Klakow, G. Welke, and W. Bauer, Proceedings of 8th Winter Workshop on Nuclear Dynamics.

FORMULATION OF PARTICLE CORRELATION AND CLUSTER PRODUCTION IN HEAVY-ION-INDUCED REACTIONS

P. Danielewicz and P. Schuck[a]

Formulas for particle correlation functions and cluster emission probabilities are derived[1] in terms of the single-particle phase-space density and production rate. The latter quantities are available from the popular dynamic models relying on nucleon degrees of freedom and nucleon-nucleon collisions. Our expressions can be used to calculate the production of $A > 2$ clusters from the dynamic models.

We start with the inclusive distribution of A free nucleons or a cluster of mass A emitted in a reaction, written in the form

$$\frac{dN_\nu}{d\nu} = \lim_{T,T'\to\infty} \frac{1}{A!}\frac{1}{TT'} \int_T^{2T} dt \int d\mathbf{x}_1 \ldots d\mathbf{x}_A \int_{T'}^{2T'} dt' \int d\mathbf{x}'_1 \ldots d\mathbf{x}'_A \, e^{iE_\nu(t-t')} \Phi_\nu^{(-)*}(\mathbf{x}_1, \ldots, \mathbf{x}_A) \times \Phi_\nu^{(-)}(\mathbf{x}'_1, \ldots, \mathbf{x}'_A) < \psi^\dagger(\mathbf{x}'_1, t') \ldots \psi^\dagger(\mathbf{x}'_A, t') \psi(\mathbf{x}_1, t) \ldots \psi(\mathbf{x}_A, t) > . \quad (1)$$

Here ν stands either for the momenta $\mathbf{p}_1, \ldots, \mathbf{p}_A$ of individual nucleons, or the center of mass momentum $\mathbf{P}$ of a cluster; $\Phi_\nu^{(-)}$ is an antisymmetrized wavefunction with outgoing boundary conditions. Using the equations of motion for the field operators ψ and $\psi^\dagger$, we transform (1) into

$$\frac{dN_\nu}{d\nu} = \frac{1}{A!} \int dt \int d\mathbf{x}_1 \ldots d\mathbf{x} \int\int dt' \int d\mathbf{x}'_1 \ldots d\mathbf{x}'_A \, e^{iE_\nu(t-t')} \Phi_\nu^{(-)*}(\mathbf{x}_1, \ldots, \mathbf{x}_A) \times \Phi_\nu^{(-)}(\mathbf{x}'_1, \ldots, \mathbf{x}'_A) < J_A^\dagger(\mathbf{x}'_1, \ldots, \mathbf{x}'_A, t') J_A(\mathbf{x}_1, \ldots, \mathbf{x}_A, t) >, \quad (2)$$

with J_A given by

$$J_A(\mathbf{x}_1, \ldots, \mathbf{x}_A) = \sum_k (-1)^{k-1} j(\mathbf{x}_k) \psi(\mathbf{x}_1) \ldots \psi(\mathbf{x}_{k-1}) \psi(\mathbf{x}_{k+1}) \ldots \psi(\mathbf{x}_A), \quad (3)$$

and

$$j(\mathbf{x}) = [\psi(\mathbf{x}), V]. \quad (4)$$

In order to obtain from (2) an expression useful for the heavy-ion reactions, we introduce the approximation

$$< J_A^\dagger J_A > \simeq \sum_\sigma \mathrm{sgn}\sigma \sum_k < j^\dagger(\mathbf{x}'_{\sigma(k)}, t') j(\mathbf{x}_k, t) > \prod_{k\neq\ell} < \psi^\dagger(\mathbf{x}'_{\sigma(\ell)}, t') \psi(\mathbf{x}_\ell, t) > . \quad (5)$$

The expectation value of the field product $< \psi^\dagger \psi >$ is simply expressed in terms of the single-particle Wigner function f, in the quasiparticle limit that underlies the dynamic models[2,3] of collisions,

$$< \psi^\dagger(\mathbf{x}', t') \psi(\mathbf{x}, t) > \simeq \int \frac{d\mathbf{p}}{(2\pi)^3} f(\mathbf{p}; \mathbf{R}, T) e^{i\mathbf{p}(\mathbf{x}-\mathbf{x}')} e^{-i\epsilon\mathbf{p}(t-t')}, \quad (6)$$

where $\mathbf{R} = (\mathbf{x}+\mathbf{x}')/2, T = (t+t')/2$, and $\epsilon_{\mathbf{p}} = \epsilon_{\mathbf{p}}(\mathbf{R}, T)$ is single-particle energy. The irreducible part of an expectation value of the single-particle source product

$$< j^\dagger(\mathbf{x}', t') j(\mathbf{x}, t) > = < j^\dagger(\mathbf{x}', t') j(\mathbf{x}, t) >_{\text{irred}} + \ldots, \tag{7}$$

containing no single-particle lines, may be identified[4] after Wigner transformation with the single-particle production rate $-i\Sigma^<$,

$$< j^\dagger(\mathbf{x}', t') j(\mathbf{x}, t) >_{\text{irred}} = \int \frac{d\omega}{2\pi} \int \frac{d\mathbf{p}}{(2\pi)^3} (-i)\Sigma^<(\mathbf{p}, \omega; \mathbf{R}, T) e^{i\mathbf{p}(\mathbf{x}-\mathbf{x}')} e^{-i\omega(t-t')}. \tag{8}$$

On using $< j^\dagger j >_{\text{irred}}$ for $< j^\dagger j >$, we get from (2), (5), (6), and (8)

$$\begin{aligned} \frac{dN_\nu}{d\nu} &= A \int dT \int d\mathbf{R}_1 \ldots d\mathbf{R}_A \int \frac{d\omega}{2\pi} \int \frac{d\mathbf{p}_1}{(2\pi)^3} \ldots \frac{d\mathbf{p}_A}{(2\pi)^3} 2\pi\delta(E_\nu - \omega - \epsilon_{\mathbf{p}_2} - \ldots - \epsilon_{\mathbf{p}_A}) \\ &\quad \times (2\pi)^3 \delta(\mathbf{P}_\nu - \mathbf{p}_1 - \mathbf{p}_2 - \ldots - \mathbf{p}_A)(-i)\Sigma^<(\mathbf{p}_1, \omega; \mathbf{R}_1, T) \\ &\quad \times f(\mathbf{p}_2; \mathbf{R}_2, T) \ldots f(\mathbf{p}_A; \mathbf{R}_A, T) g_\nu(\tilde{\mathbf{p}}_1, \ldots, \tilde{\mathbf{p}}_{A-1}; \tilde{\mathbf{R}}_1, \ldots, \tilde{\mathbf{R}}_{A-1}). \end{aligned} \tag{9}$$

Here g_ν is the Wigner function of the state ν, and tilde indicates the Jacobi coordinates and conjugate momenta. The production rate in the kinetic models is[4]

$$\begin{aligned} -i\Sigma^<(\mathbf{p}, \omega; \mathbf{R}, T) &= \int \frac{d\mathbf{p}_1}{(2\pi)^3} \frac{d\mathbf{p}'}{(2\pi)^3} \frac{d\mathbf{p}'_1}{(2\pi)^3} (1 - f(\mathbf{p}_1; \mathbf{R}, T)) f(\mathbf{p}'; \mathbf{R}, T) f(\mathbf{p}'_1; \mathbf{R}, T) \mid \mathcal{M}_{NN \to NN} \mid^2 \\ &\quad \times 2\pi\delta(\omega + \epsilon_{\mathbf{p}_1} - \epsilon_{\mathbf{p}'} - \epsilon_{\mathbf{p}'_1}) (2\pi)^3 \delta(\mathbf{p} + \mathbf{p}_1 - \mathbf{p}' - \mathbf{p}'_1). \end{aligned} \tag{10}$$

The rate in (9) is evaluated off the energy shell. Following a collision the nucleon is off-shell and may form a cluster with other nucleons. The other nucleon in the nucleon-nucleon collision, c.f. eq. (10), acts as a catalyzer permitting the energy and momentum to be conserved.

As it stands, eq. (9) does not include the possibility of absorption due to further interactions following the production. This can be accounted for by summing up the other terms on the r.h.s. of eq. (7). The final expression is a generalization of eq. (9),

$$\begin{aligned} \frac{dN_\nu}{d\nu} &= A \int dt \int d\mathbf{x}_1 \ldots d\mathbf{x}_A \int dt' \int d\mathbf{x}'_1 \ldots d\mathbf{x}'_A \chi_\nu^{(-)*}(\mathbf{x}_1, \ldots, \mathbf{x}_A, t) < j^\dagger(\mathbf{x}'_1, t') j(\mathbf{x}_1, t) >_{\text{irred}} \\ &\quad \times < \psi^\dagger(\mathbf{x}'_2, t') \psi(\mathbf{x}_2, t) > \ldots < \psi^\dagger(\mathbf{x}'_A, t') \psi(\mathbf{x}_A, t) > \chi_\nu^{(-)}(\mathbf{x}'_1, \ldots, \mathbf{x}'_A, t'). \end{aligned} \tag{11}$$

The wavefunction $\chi_\nu^{(-)}$ satisfies a more general equation than $\Phi_\nu^{(-)}$, by inclusion of the time-dependent complex optical potential for nucleons.

Our results have been obtained without any reference to ad hoc quantities. The implementation of our expressions into dynamic codes may be perturbative, or with a feedback, for composites, onto

the reacting system. From eq. (11) the Koonin formula[5] can be derived,[1] and that derivation is more fundamental, in our opinion, than the one given in previous work.[6] Equation (2) can be used to justify the temperature determination from resonance yields.

a. Institut des Sciences Nucleaires, 53 Avenue des Martyrs, 38026 Grenoble Cedex, France

References

1. P. Danielewicz and P. Schuck, Phys. Lett. B 274, 268 (1992).
2. J. Cugnon, Phys. Rev. C22, 1885 (1980).
3. G. F. Bertsch, S. Das Gupta, and H. Kruse, Phys. Rev. C29, 673 (1984).
4. P. Danielewicz, Ann. Phys. (N.Y.) 152, 239 (1984).
5. S. E. Koonin, Phys. Lett. 70B, 43 (1977).
6. W. G. Gong, W. Bauer, C. K. Gelbke, and S. Pratt, Phys. Rev. C 43, 781 (1991).

FORMATION OF COMPOSITES EMITTED AT LARGE ANGLES IN INTERMEDIATE AND HIGH ENERGY REACTIONS

P. Danielewicz

We examine the importance of the nuclear mean-field potential, elementary collisions, and the Coulomb potential, for the formation of composites emitted at large angles in nuclear reactions.[1] We demonstrate that the nucleon-nucleon collisions are by far most essential in the formation of high-energy composites. A model with composite formation in the elementary collisions is applied to the intermediate-energy heavy-ion reactions.

The process of composite formation, running backward in time, becomes a breakup process that may be easier to consider than the process of formation. Either the formation or breakup require an external agent. For the breakup or formation by the nuclear mean-field potential, the second derivative of the potential must be finite, or, correspondingly, the force must vary over the region occupied by a composite. A potential changing linearly with position and giving a constant force could only accelerate a composite as a whole. The Coulomb potential is weak even for heavy nuclei, but it is long range and the force acts only on protons making it easier to change the internal state of a composite. The interaction with individual nucleons is of short range and thus constituents of a composite are separately affected. Respectively, the interaction is effective in the formation and breakup, except at low energies when the collisions with individual nucleons are suppressed by the Pauli principle.

We illustrate our points by carrying out calculations of deuteron breakup in the Glauber model. Figure 1 shows contributions to the breakup cross sections from different impact parameters $d\sigma/db$, for 100 MeV/nucleon deuterons incident on ^{9}Be. At this and higher energies we find that nuclear mean-field plays quite insignificant role in the breakup. We relate the deuteron formation to breakup by considering uniform fluxes of protons and neutrons incident on the target nucleus which catalyzes the formation. Using microscopic reversibility the number of transitions with the deuteron formation can be made proportional at high energies in such situation, to the cross section for breakup on the same target nucleus.[1] Thus we can conclude that the mean field does not play a role in the composite formation either, at high energies.

The formation of deuterons in high energy reactions was attributed to the mean field in the model by Butler and Pearson.[2] We analyze their model and show that these authors were able to reproduce data from proton induced reactions, by using the Born approximation that does not apply to the nuclear

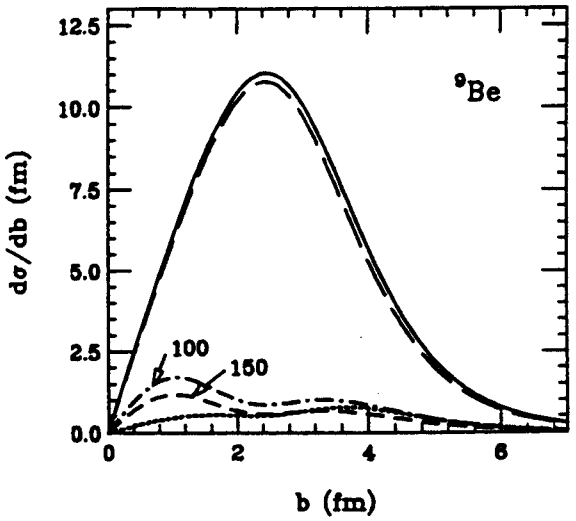

Figure 1: Contributions to the breakup cross sections from different impact parameters $d\sigma/db$, in the Glauber approximation, for deuterons incident on ^{9}Be. Except for the lines marked 150 that refer to 150 MeV/nucleon, all results are for the incident energy of 100 MeV/nucleon. The solid and long-dashed lines show results obtained including mean field and collisions and solely collisions, respectively. The short-dashed and dash-dotted curves are obtained including only mean field potential. The dotted lines represent contributions to the elastic breakup cross section.

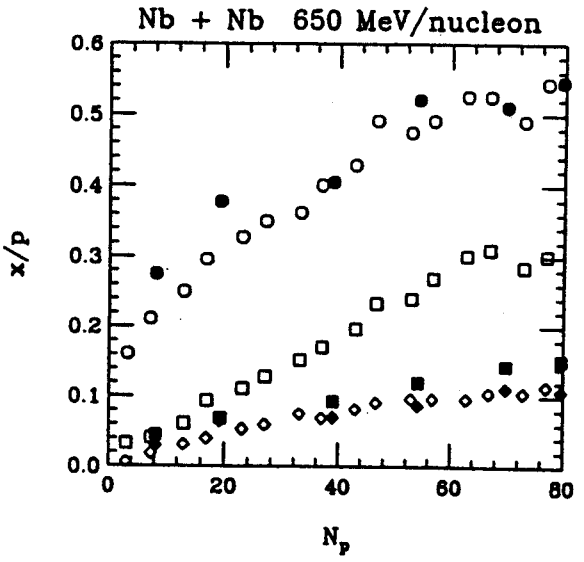

Figure 2: Ratios of composite yields to proton yields x/p as a function of the participant proton multiplicity N_p. The circles, squares and diamonds indicate, respectively, the d/p, t/p and ^{3}He/p ratios. The measured values are shown with open symbols, and the calculated ones with the filled symbols.

potential, and by overestimating by about one order of magnitude the number of neutron-proton pairs that can contribute to deuteron production.[1]

A transport model with deuteron,[3] triton and helion production in elementary collisions, based on the above considerations, is applied to the heavy-ion reactions. Figure 2 compares the particle yield ratios calculated in the model as a function of participant proton multiplicity, with the data[4] of the Plastic Ball group for the Nb + Nb reaction at 650 MeV/nucleon. It is seen that we can reproduce the d/p and ^{3}He/p ratios, but not t/p. Unlike the measurements, our $t/^3$He ratios are roughly consistent with N/Z for the system. Comparison with other results of the Plastic Ball group for composite particles, in particular the mean transverse energies, is forthcoming.

References

1. P. Danielewicz, Report MSUCL-832, Proc. Int. Workshop on Dynamical Fluctuations and Correlations in Nuclear Collisions, Aussois, France, 1992.
2. S. T. Butler and C. A. Pearson, Phys. Rev. 129, 836 (1963).
3. P. Danielewicz and G. F. Bertsch, Nucl. Phys. A533, 712 (1991).
4. K. G. R. Doss *et al.*, Phys. Rev. C37, 163 (1988).